Experimental study of spinon-phonon coupling in spin-chain cuprates

David Msika, Dalila Bounoua, Olivier Demortier, Françoise Damay, Romuald Saint-Martin, Rolf Heid, Alexandre Ivanov, Andrea Piovano, Frédéric Bourdarot, David Bérardan, et al.

Experimental study of spinon phonon coupling in spin chain cuprates

David Msika,[1,*] Dalila Bounoua,[2,†] Olivier Demortier,[2] Françoise Damay,[2] Romuald Saint-Martin,[3] Rolf Heid,[4] Alexandre Ivanov,[5] Andrea Piovano,[5] Frédéric Bourdarot,[6] David Bérardan,[3] Loreynne Pinsard-Gaudart,[3] and Sylvain Petit[2,‡]

[1] *Institut de Chimie Moléculaire et des Matŕiaux dOrsay (UMR CNRS 8182), Université Paris-Saclay, F-91405 Orsay, France*
[2] *Laboratoire Léon Brillouin, CEA-CNRS UMR12, CEA, CNRS, Université Paris-Saclay, 91191 Gif sur Yvette Cedex, France*
[3] *Institut de Chimie Moléculaire et des Matériaux dOrsay (UMR CNRS 8182), Université Paris-Saclay, F-91405 Orsay, France*
[4] *Institute for Quantum Materials and Technologies, Karlsruhe Institute of Technology, 76021 Karlsruhe, Germany*
[5] *Institut Laue langevin, 6, rue Jules Horowitz, BP 156 F-38042 Grenoble, France*
[6] *Université Grenoble Alpes, CEA, IRIG, MEM, MDN, F-38000 Grenoble cedex, France*

In this paper, we focus on the thermal transport properties of antiferromagnetic spin chains cuprates. The chain magnetic excitations, the spinons, partake in heat transport at low temperature, but spinon heat transport decays well below room temperature, possibly because of a coupling with phonons. By means of inelastic neutron scattering, we thoroughly study the lattice dynamics of spin chain compounds Sr_2CuO_3, Ca_2CuO_3, along with double spin-chain compounds $SrCuO_2$. We come to the conclusion that there are no obvious anomalies in the phonon dispersions, which suggests a weak spinon-phonon coupling regime.

PACS numbers:

I. INTRODUCTION

The thermal properties of spin liquids and more generally of unconventional magnets attracted much attention over the last decade [1]. For instance, cuprate spin chains exhibit amazing heat transport properties, with an exceptionally high heat conductivity κ along the spin chain axes [2, 3]. While these properties open up prospects such as the design of specific devices to dissipate heat in High-Frequency electronics, they also raise fundamental questions.

In such insulating materials, the heat current is expected to be carried by both phonons and magnetic excitations, hence the heat conductivity along the spin chain axis reads $\kappa = \kappa_{ph} + \kappa_{mag}$. While the phononic part has been studied for a long time, the magnetic part κ_{mag} is under intense scrutiny. In ladder-compounds such as $Sr_{14}Cu_{24}O_{41}$, phononic and magnetic contributions are easily disentangled, as they do not peak in the same temperature region [4–6]. However those conductivity peaks overlap in cuprates XXZ spin-chain compounds, such as $SrCuO_2$, Sr_2CuO_3 and Ca_2CuO_3. Then, a workaround to isolate and study κ_{mag}, is to subtract the heat conductivity perpendicular to the spin chains, as in this direction the heat conductivity is believed to be solely phononic, hence $\kappa_{mag} = \kappa_{\parallel} - \kappa_{\perp}$. This method was first suggested in the study of the heat conductivity of $KCuF_3$, which is also an XXY Heisenberg spin chain realisation [7]. Following this method, $SrCuO_2$ is found to exhibit a strong κ_{mag}, that peaks at about 600 Watt/m.K at 37 K, a value comparable to the one found in copper for instance [8–12]. Current interpretation assumes that this heat flow is carried by spinons, the fractionalized magnetic excitations typical of the 1D antiferromagnetic Heisenberg model [13, 14]. κ_{mag} is thus a direct manifestation, at a macroscopic scale, of the quantum nature of those 1D chains.

These thermal properties are also accompanied by a hidden fragility, as a small perturbation of the spin chain may interfere with, and eventually hinder, the magnetic contribution to heat transport. It was shown [15] in $SrCuO_2$ indeed that 1% Nickel doping on the Cu site opens a gap in the spinon continuum. This spin pseudogap depletes available magnetic states for heat transport, which explains the loss of the thermodynamic properties upon doping. Different other substitutions were attempted in $SrCuO_2$, with S=0 3d ions on the Cu^{2+} site. To allow such substitutions, the dopant's ionic radius needs to be close to the copper's. Due to stringent solubility limit, only 1% of those dopants could be systematically inserted in the Cu chain. Doping with Mg and Zn lead to the same effect of spin chains segmentation, and opens a spin pseudogap of about 6.9 meV [16].

Experimentally, the thermal conductivity κ_{mag} of $SrCuO_2$ is found to collapse above about 50 K [3, 12, 17]. Pure as well as doped compounds show the same behaviour in this temperature range, suggesting that this rapid drop of κ_{mag} as temperature increases is an intrinsic effect, independent of the presence of defects. Current understanding argues that this behaviour is due to growing scattering rate of spinons by phonons [12].

Phonons can indeed behave as scattering centers for spinons, and vice versa. Due to the very large antiferromagnetic exchange coupling J_{AF} between Cu^{2+}, about

* david.msika@universite-paris-saclay.fr
† dalila.bounoua@cea.fr
‡ sylvain.petit@cea.fr

2000 K, spinons' velocity is far greater than phonons', which can therefore be considered as static defects. By severing the spin chain, they effectively limit spinon mean free path along the chain, thus reducing heat transport. In prior works, spinon inverse mean free path was fitted by the form $\ell^{-1} \sim g^2/J\ T\ e^{-\omega^*/T}$, inspired by phonon-mediated Umklapp scenario [18], where g is the spin-phonon coupling constant and ω^* a typical optical phonon energy, yet, this analysis led to an intriguingly strong spin-phonon interaction $g \approx 1$ (see also appendix A).

In a recent theoretical study, Chernyshev *et al.* [19] proposed a novel approach and derived a microscopic spin-phonon scattering rate where phonons act as thermally populated defects for the fast spin excitations. The inverse mean free path is found to exhibit a distinctive temperature dependence $\ell^{-1} \sim g^2 J/T \frac{1}{\sinh \omega_o/T}$, the $1/T$ prefactor being strongly reminiscent of the result for scattering on weak impurities. Interestingly, the authors argue that only a weak coupling constant is necessary to explain the data, unlike the previous scenario, and which calls for the strong coupling limit.

To shed light on this issue, it is natural to study the phonon dispersions, to determine whether they exhibit anomalous behavior as a function of temperature and/or upon crossing the spinon spectrum, in order to constrain experimentally the spinon-phonon coupling in those cuprates. The present study addresses this issue. We report inelastic neutron scattering data, the technique of choice to reveal both phonons and spinons spectra in (Q, ω) space, which strongly advocates for the weak coupling picture.

This paper is organized as follows. The first section is devoted to the description of methods and experimental techniques. In the second section, we present the phonon spectra, as observed by means of inelastic neutron scattering, before turning to the discussion in a third part and coming to the conclusions. In the appendix, we present additional information about calculations of κ_{mag} in the two different approaches mentioned above and discuss the consequence of the Pd^{2+} substitution at the Cu^{2+} site (an $S = 0$ impurity slightly larger that Cu^{2+}). This data provides a novel example showing that doping causes the opening of a pseudo gap in the two-spinon continuum.

II. METHODS

The single crystals were grown using the Traveling Solvent Floating Zone Method (CSI Optical furnace FZ-T-10000-H-VII-VPO-PC) [20, 21]. Samples were characterized by magnetic susceptibility measurements carried out on a SQUID magnetometer (Quantum Design MPMS 5). A DC magnetic field of 1000 Oe was applied along and perpendicularly to the spin chain axis, c^* and a^* respectively. Heat capacity measurements were also carried out on an PPMS (Physical Property Measurement System), Quantum Design 9T. The measurements were performed using the adiabatic method, which measures the thermal dissipation of the sample towards a temperature reservoir. This method is both fast and precise, and is only limited by the sample weight measurement accuracy. The sample was kept in a vacuum of 0.01 mTorr, and protected by an anti-radiation shield, to prevent dissipation from convection and thermal radiation respectively. An Apiezon N grease was used to ease the heat transfer from the sample to the sample holder, and their contribution to C_p was calibrated. These measurements of the thermodynamic properties of the spin chain compounds are to be found in the appendix of this article. We further describe the structure of the compounds, and the directions measured by the inelastic scattering measurements.

$SrCuO_2$ crystallizes in the orthorhombic space group *Cmcm*. The spin chains are formed by alternating Cu-O-Cu ions along the c-axis with nearly 180 degrees bonding angles. The Cu^{2+} ions are square planar coordinated within the CuO_4 plaquettes contained in the (b, c) plane, and the whole structure can be described as alternating stacks of ribbons of zigzag Cu-O chains, along $(H00)$ and $(0K0)$, separated by Sr atoms along $(0K0)$. In a similar fashion, both Sr_2CuO_3 and Ca_2CuO_3 crystallise in the orthorhombic space group *Immm*. The spin chains are formed by a 180 degrees bond between Cu-O-Cu ions in the structure, aligned along the $(0K0)$ direction instead. This bond is the building block of strong superexchange of about $J_{AF}/k_B \approx$ 2000 K between half-integer Cu^{2+} spins. In the following, we refer to the spin chain axis to be $(00L)$ in $SrCuO_2$ and $(0K0)$ in both Sr_2CuO_3 and Ca_2CuO_3.

For INS measurements, the sample was then glued with fluorine glue on an aluminum cold finger, to have the (b, c) plane as the scattering plane for Sr_2CuO_3 and Ca_2CuO_3, and the (a, c) plane as the scattering plane for $SrCuO_2$. The sample was mounted in a closed cycle displex, capable to reach temperatures as low as 3K. The neutron measurements were carried out with constant wave-vector k_F=2.662 Å^{-1} on the thermal neutron triple-axis spectrometers 2T installed at LLB-Orphée (France), IN8 and IN12 (CRG-CEA instrument) [22–24], both installed at the Institut Laue Langevin (France). This final wavevector was chosen as its harmonics are suppressed by the PG002 graphite filter and yield energy resolution of about 1 meV at zero energy transfer. Open collimations were used, and the curvature of the monochromator and graphite analyzer were set to maximize the flux at the sample during the experiment. The sample crystallographic orientation was found using the Laue method, in a back-scattering geometry.

We show on Fig.1 the calculated 2-spinons continuum (measurements are reported in Ref. [25]). In the pure compounds, it goes soft at half integer positions along the spin chain direction, whereas in the doped materi-

als, the chains segmentation by impurities gives rise to the opening of spin pseudogaps at the same positions. Furhermore, owing to the huge value of J, it is worth noting the discrepancy between the spinon and the phonon typical energies, highlighted by Fig.1a and b): the former dwarfs the latter, hence, in the 0-50 meV range, the 2-spinons continuum appears as thin vertical lines. Phonons can then be considered as low energy scatterers to the highly dispersive spinons. Lines where the 2-spinons continuum goes soft in the scattering plane are indicated by red dotted lines in Fig.1c). As the magnetic form factor decreases with the momentum exchange Q, it is best observed as close as possible from the origin of the reciprocal space. To measure phonons, one should take advantage of the $(Q.e_s)^2$ term comprised in the phonon cross-section (e_s is the polarization of mode s). Fig.1c) shows the appropriate scanning directions in the scattering plane to probe transverse and longitudinal modes propagating perpendicular to the chain (orange and green respectively), as well as transverse and longitudinal modes propagating along the chain (blue and magenta respectively). Because of the Q^2 dependence it is also appropriate to measure the spectrum at large momentum transfer.

Those phonon measurements in $SrCuO_2$ were confronted to a calculation of the phonon dispersion using density-functional perturbation theory (DFPT) [26] in the framework of the mixed-basis pseudopotential method [27, 28]. Norm-conserving pseudopotentials of Vanderbilt-type [29] were combined with a mixed-basis expansion of the valance states consisting of plane waves up to kinetic energy of 25 Ry and local functions of s, p type for O and s, p, d type for Sr and Cu, respectively, to account for the more localized components of the valence states. The exchange-correlation functional was treated in the local-density approximation [30], and Brillouin-zone integration was performed with an orthorhombic $16 \times 4 \times 16$ k-point mesh. For the $Cmcm$ structure of $SrCuO_2$, experimental lattice constants ($a = 3.58$ Å, $b = 16.33$ Å, $c = 3.92$ Å) were used, while internal structural parameters were relaxed. The phonon dispersion was then obtained by performing DFPT calculations of dynamical matrices on a $2 \times 2 \times 8$ momentum mesh, i. e. denser along the spin direction, and subsequent applying standard Fourier interpolation to approximate dynamical matrices throughout the Brillouin zone.

III. PHONON SPECTRUM

To investigate the weak/strong coupling issue and shed light on transport properties, the phonon spectra in $SrCuO_2$, Sr_2CuO_3 and Ca_2CuO_3 have been investigated by means of inelastic neutron scattering. We studied at length the longitudinal and transverse phonons branches dispersing along and perpendiculary to the chains direction in the three compounds. This study was complemented by DFT calculations in the case of $SrCuO_2$,

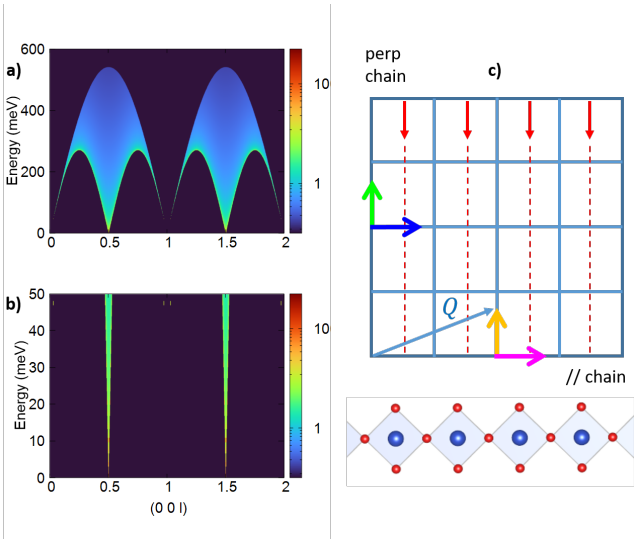

FIG. 1. a) and b) display the calculated 2-spinon continuum in different energy ranges, using the full scale in a) up to 600 meV, because of the high value of J_{AF} (=2600 K in the calculation shown); and up to 50 meV in b) to compare with the typical energies of phonon modes. c) shows a sketch of the reciprocal space probed in the present neutron scattering experiments. The plane is spanned by the direction of the spin chains (c axis in $SrCuO_2$, b axis in Sr_2CuO_3 and Ca_2CuO_3) and a perpendicular direction (a axis in $SrCuO_2$, c axis in Sr_2CuO_3 and Ca_2CuO_3). The red arrows which terminate as dotted lines indicate the zone boundaries where the two-spinons continuum goes soft. Orange (resp green) arrows show the scan directions allowing to probe transverse (resp longitudinal) phonon modes propagating perpendicular to the chains. Blue (resp magenta) arrows show the directions to probe transverse (resp longitudinal) phonon modes propagating along the chains.

from which we determined the dynamical structure factor. The aim was, by comparing experimental and calculated dynamical structure factors, to track any possible hint for a coupling between the two types of quasiparticles, e.g. temperature change or lineshape broadening on crossing the 2-spinons continuum, especially in the region of (Q, ω) space occupied by both dynamical responses. For instance, a phonon line-width broadening could show that phonon lifetimes are decreasing, after scattering with spinons.

On Fig.2 and Fig.3, we show representative phonon spectra propagating respectively perpendicular (green and orange directions in Fig.1) and along the spin chains (blue and magenta directions in Fig.1). On Fig.2, the scans do not cross the 2-spinons continuum, which is thus not visible. In contrast, in Fig.3, the 2-spinons continuum appears as a faint intensity (marked by red arrows) at $(2, 0, \frac{1}{2})$ in $SrCuO_2$ or $(0, \frac{1}{2}, 2)$ in Sr_2CuO_3 and Ca_2CuO_3. The spinon dispersion is so steep that it appears as a straight line in this energy range.

In the three compounds, the phonon dispersions show a striking similarity with one another, as expected as

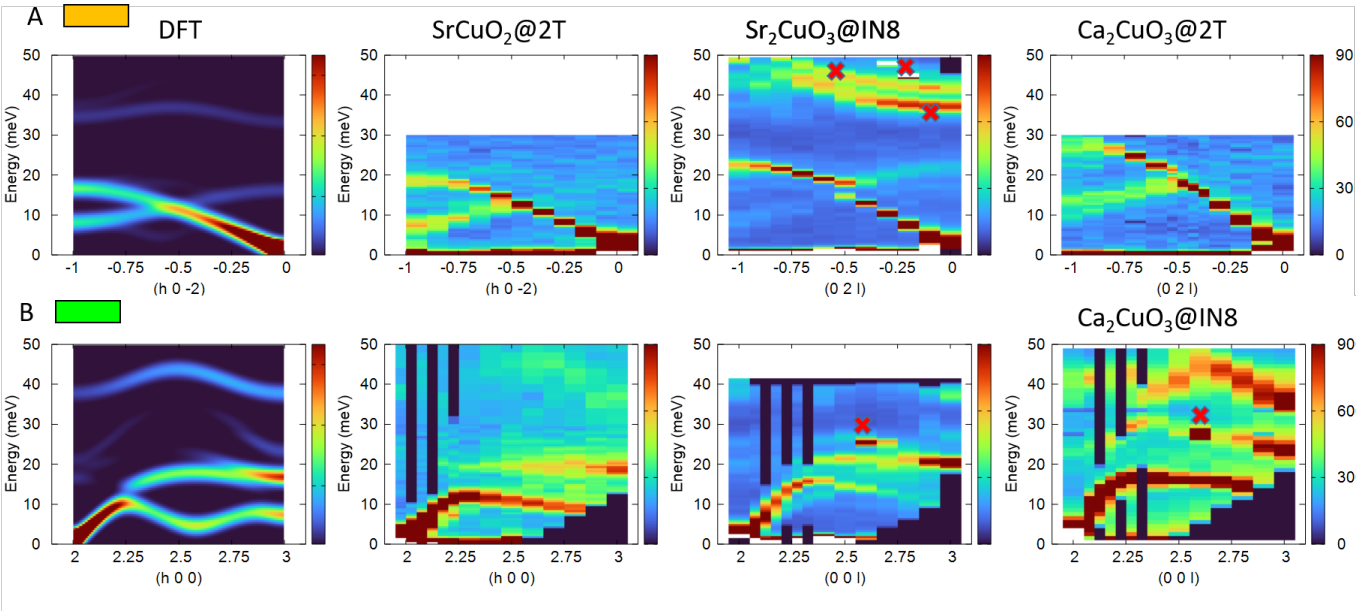

FIG. 2. Phonon modes propagating perpendicular to the spin chains in $SrCuO_2$ at 4 K, Sr_2CuO_3 at 9 K and Ca_2CuO_3 at 15 K. Row A (resp B) shows transverse (resp longitudinal) modes. Each row is labeled by an orange (resp green) rectangle, referring to the colored arrow in the sketch of Fig. 1. DFT calculations performed for $SrCuO_2$ are also shown for comparison. Red crosses indicate spurious scattering that we could unambiguously identify. These are due to contamination either from the aluminum powder rings coming from the sample holder or to elastic incoherent scattering on the samples, both appearing at a finite energy because of an insufficient filtering. In the former case, the spurious scattering forms a line, while in the second it gives rise to a "hot spot". These are unfortunately unavoidable on thermal spectrometers. Note that the maximum of color scale is the same for a given sample but depend on the spectrometer where the data was taken.

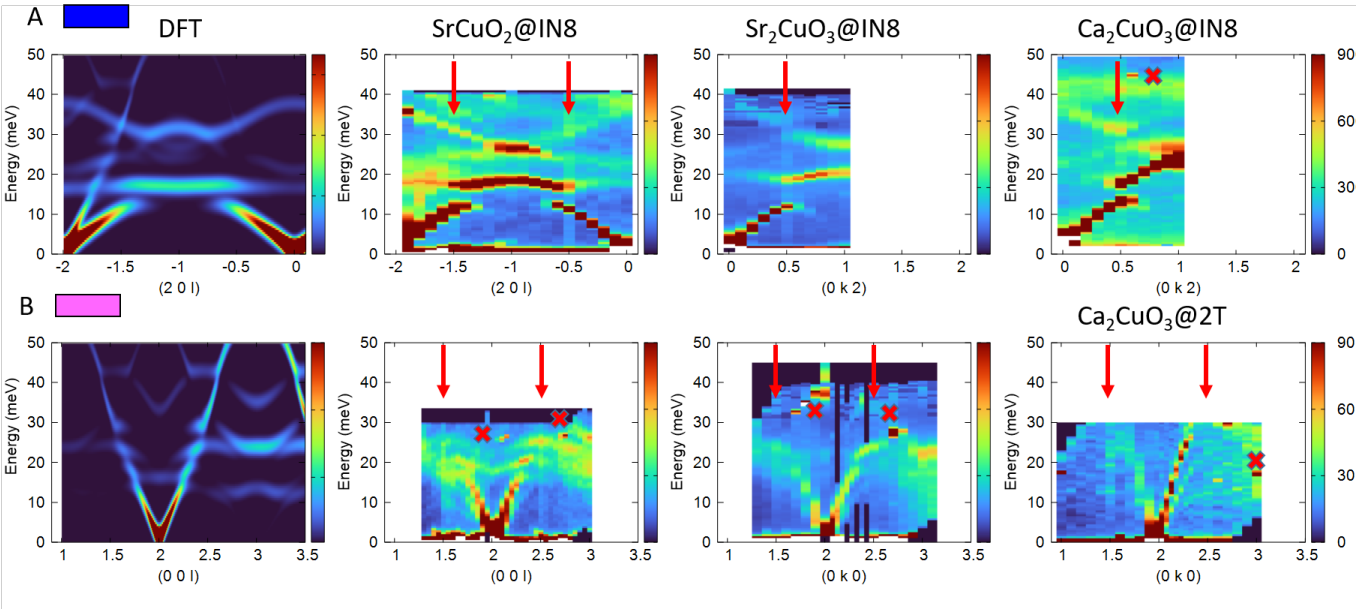

FIG. 3. Phonon modes propagating perpendicular to the spin chains in $SrCuO_2$ at 4 K, Sr_2CuO_3 at 9 K and Ca_2CuO_3 at 15 K. Row A (resp B) shows transverse (resp longitudinal) modes. Each row is labeled by a blue (resp magenta) rectangle, referring to the colored arrow in the sketch of Fig. 1, see also Fig 2.

they have closely related crystal structures. The typical energies of the phonons are however larger as the heavier Sr cation in Sr_2CuO_3 is replaced by lighter calcium to get Ca_2CuO_3.

The main characteristic of the spectra is the existence of a series of avoided crossings between acoustic branches and nearly flat optical modes. For example, the longitudinal acoustic phonon propagating along the chains (Fig. 3) avoids crossing with a flat optical branch of symmetry B_{3u}, at energy 17 meV in $SrCuO_2$ 19.8 meV at (0,0,2) in Sr_2CuO_3 and 23.6 ± 1.4 meV at (0,1,2) in Ca_2CuO_3. After the avoided crossing, the transverse acoustic branch fades in the background. The same behaviour is also particularly remarkable for the transverse acoustic mode propagating perpendicular to the chains (Fig. 2), with a small gap at $(-\frac{1}{2}, 0, -2)$ in $SrCuO_2$ and $(0, 2, -\frac{1}{2})$ in Sr_2CuO_3 and Ca_2CuO_3. The spectral weight jumps to the upper branch, while the lower one goes soft down to about 10 meV at the zone boundary. This low energy indicates some weakness of the bonds along specific directions, which remains to understand.

The DFT simulation closely matches the experimental phonon spectrum of $SrCuO_2$ and accurately predicts the avoided crossing between the acoustic branch and optical phonons. Spectral weight evolution of the phonon modes throughout the Brillouin zone is also quite well reproduced by the DFT calculations.

Furthermore and within the experimental resolution, there is no clear evidence for a peculiar behavior at the crossing points between optical phonons and the 2-spinons continuum. The spectral weight of the different branches, as well as the dispersions, are monotonous and regular, without any anomaly as they cross the magnetic spectrum. In Ca_2CuO_3, we looked in particular for the longitudinal phonons suspected to couple with the spinons as argued by Chen *et al.* [17], with energy 25.6 meV and 78.6 meV at the gamma point. While we could confirm with inelastic neutron scattering the presence of a mode at about 25 meV. The second mode could not be easily confirmed for technical reasons, as the resolution function worsens too much. This is all the more unfortunate that the spin-phonon coupling is probably stronger with the higher energy mode, as suggested in [19].

Finally, looking for a possible evolution with temperature, spectra were further measured for the three samples, at Q corresponding to crossings with the 2-spinons continuum, and at different temperatures relevant to the heat transport: below the conductivity peak, in the temperature region of maximum conductivity, and above. These spectra were fitted by the sum of Gaussian profiles centered on the phonon energies and with intensities corrected for the detailed balance factor, on top of a linear background. Fig. 4 illustrates the result of this analysis. It displays the energies and intensities of the phonons at Q=$(0, 0, 2.5)$ (longitudinal configuration) in $SrCuO_2$ and at Q=$(0, 0.5, 2)$ (transverse configuration) in Sr_2CuO_3 and Ca_2CuO_3. Note that the error bar of the energies is actually not the corresponding uncertainty but the fitted FWHM. No significant softening, hardening, nor evolution of the width can unambiguously detected. A weak temperature dependence of the intensities can be noticed but nothing that would go beyond expected

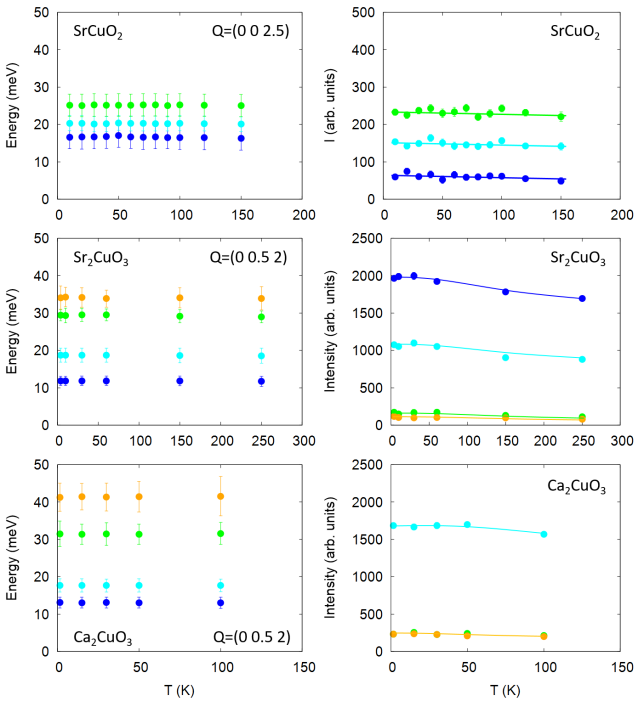

FIG. 4. Temperature evolution of the phonon energies (left) and intensities (right) in $SrCuO_2$, Sr_2CuO_3 and Ca_2CuO_3. Error bars actually depict the FWHM of each mode, being essentially due to the experimental resolution. Lines are guides to the eyes. In the pure harmonic approximation, the intensities are expected to be temperature independent. $SrCuO_2$ data should be confronted to row B in Fig. 3 (with modes at around 17, 20 and 25 meV. Sr_2CuO_3 and Ca_2CuO_3 data should be confronted to row A in the same figure (with modes at around 12, 20, 29 and 33 meV).

an-harmonic effects. Here we may suggest a future experiment, using inelastic Xray scattering, which has a constant and better resolution compared with thermal neutron scattering at such a high energy exchange [31], to seek for a possible broadening of the phonon modes.

IV. DISCUSSION

It is thus very difficult to highlight any anomaly in the phonon spectra, which suggests that the microscopic spin-phonon coupling is weak, as pointed out by Chernychev *et al.*

This is all the more intriguing that a small substitution on the copper site is known to have a strong impact, opening a gap in the 2-spinons continuum (see Appendix B for neutron results on Pd-doped samples). Furthermore, there are direct manifestations of the spinon phonon coupling: Ref. [17, 32] report that 2-phonons excitations in Ca_2CuO_3, typically in the 1400 cm^{-1} range (170 meV) do exhibit an asymmetric Fano line-shape. According to DFT calculations which show that the maximum energy of the optical phonons is of the order of 80

meV, these excitations correspond to pairs of such high energy optical phonons. Interestingly, however, the lower energy features, in particular the 1-phonon excitations do apparently have a normal profile and we note that this is consistent with our neutron scattering measurements.

Further relevant experimental information for this discussion is reported in Ref. [32], which considers the spin-Peierls compound $CuGeO_3$. In this other 1D spin chain, it is well known that the spin-lattice coupling is large enough to cause a dimerization of the chain. Unconventional magnetic excitations emerge, consisting in a dispersing magnon mode above a gap Δ_{SP} along with a continuum above $2\Delta_{SP}$ [33]. Sugai *et al* show that below the spin-Peierls transition, due to the structure transition, six new peaks appear in the Raman spectra at 30, 60, 105, 228, 370 and 819 cm^{-1}. The peaks which are within the magnetic continuum are asymmetric, while the outside peak at 819 cm^{-1} remains symmetric. As a result, the spin-phonon coupling apparently generates the Fano line-shape, provided the phonons energies are comparable to the magnetic continuum s energy. Because of the extremely large value of J in $SrCuO_2$, Sr_2CuO_3 and Ca_2CuO_3, the optical phonon remain very far from the energy range of the spinon continuum. Hence, the asymmetric line-shape would not manifest for the 1-phonon modes but on 2-phonons excitations (at 170 meV in Ca_2CuO_3), which have an energy large enough to fall within the magnetic continuum. This reasoning, however, is not true, at zone centers and zone boundaries, where the 2-spinons continuum goes soft, hence entering the phonon energy range. We shall argue that the spinon density of states remains small in this Q-range, thus, even if the spin-phonon coupling exists, it could be not very efficient.

V. CONCLUSION

In this paper, we looked for the manifestation of a spin-phonon coupling on the excitation spectra of spin chains $SrCuO_2$, Sr_2CuO_3 and Ca_2CuO_3. Results tend to favor a scenario in which the spin-phonon coupling remains weak. Moreover, this is consistent with recent theoretical approaches [19], hence giving support to the proposed spin-phonon relaxation rates with which the magnetic contribution should be modeled. So far, the spinon contribution to heat conductivity was obtained from a difference between the conductivity in the spin chain direction minus the perpendicular. However, this assumption is questionable. For instance, our INS measurements also show that the sound velocities are not isotropic, which leads us to believe that the phonon conductivity tensor is not isotropic either, while it is the fundamental hypothesis to the approach proposed by Miike *et al.* [7]. Using the DFT calculation, and thus the whole lattice response, to better evaluate this tensor seems a fruitful endeavour for further research, which would allow better extraction of spinon contribution to the heat conductivity.

Acknowledgements: D.M., S.P., D.B., F.D. and O.D. acknowledge financial support from the 2FDN (french neutron scattering society). All authors thank Ketty Beauvois for her assistance with the Orient-Express Laue instrument, which facilitated the experiments on IN8. D. M also thanks Emilie Amzallag for fruitful discussions on phonon mode symmetries.

Appendix A: Weak and strong coupling regimes

The magnitude of the spin-phonon coupling was originally evaluated based on the analysis of thermal conduction data. $SrCuO_2$, Sr_2CuO_3 and Ca_2CuO_3 are known to have a highly anisotropic heat conduction, depending on whether the heat flux flows along the direction of the chains, or perpendicular to the chains. The prevailing analysis today is to determine the magnetic contribution by taking the difference between these measurements. Using the Boltzmann equation, one can write an approximate simple expression for the magnetic contribution [8–12] :

$$\kappa_{mag} = \frac{\pi}{3} n_s \frac{k_B}{\hbar}\ k_B T\ \ell \tag{A1}$$

where n_s is the number of chain per unit area, k_B is the Boltzmann constant, and ℓ is the spinon mean free path. Strikingly, its temperature dependence strongly impedes the expected increase of κ_{mag} due to the $k_B T$ linear term. In prior works, κ_m was fitted assuming ℓ^{-1} given by:

$$\ell^{-1} = \frac{1}{\ell_o} + \frac{g^2}{c}\frac{T}{J}\ e^{-\omega^*/T} \tag{A2}$$

a formula inspired by phonon-mediated Umklapp scenario [18]. ℓ_o is an average length of a defect-free chain segment, $1/\ell_o = n_d$, where n_d is the concentration of these defect, c is the Cu-Cu distance, g the dimensionless spin phonon coupling constant and ω^* a typical optical phonon energy.

In a recent theoretical study, Chernyshev *et al.* [19] proposed a novel approach and derived a microscopic spin-phonon scattering rate where phonons act as thermally populated defects for the fast spin excitations. The authors find a new temperature dependence for the inverse mean free path due to 1 phonon scattering:

$$\ell^{-1} = \frac{1}{n_d} + \frac{2g_{1\mathrm{ph}}^2}{c}\frac{J}{T}\ \frac{1}{\sinh \omega^*/T} \tag{A3}$$

the $1/T$ prefactor being reminiscent of the result for scattering on "weak impurities". For T above $\sim \omega^*$, the mean-free path saturates at $\ell^{-1} \sim \frac{2g_{1\mathrm{ph}}^2}{c}\frac{J}{\omega^*}$ hence other temperature dependent terms may become important. Ref. [19] argues that in this regime, an additional contribution due to 2-phonons scattering should be taken into account, leading to:

$$\ell^{-1} = \frac{1}{n_d} + \frac{g_{2\mathrm{ph}}^2}{c}\frac{J}{T}\ \frac{\cosh \omega^*/T}{\sinh^2 \omega^*/T} \tag{A4}$$

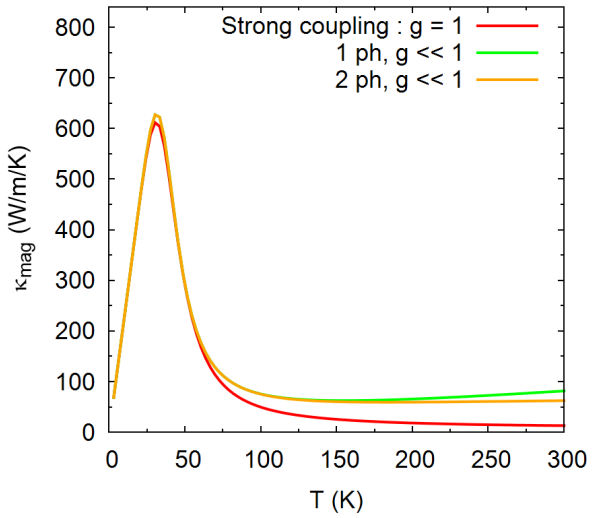

FIG. 5. Thermal conductivity κ_{mag} calculated from Eq. A1. Different models for the mean free path are envisaged. For the Umklapp-like mean free path, we use $g = 1$, $\omega^* = 204$ K. For the weak coupling limit, we use g =0.025, $\omega^* = 300$ K. In all calculations, $n_d = 35.10^{-7}$ and $J = 2600$ K.

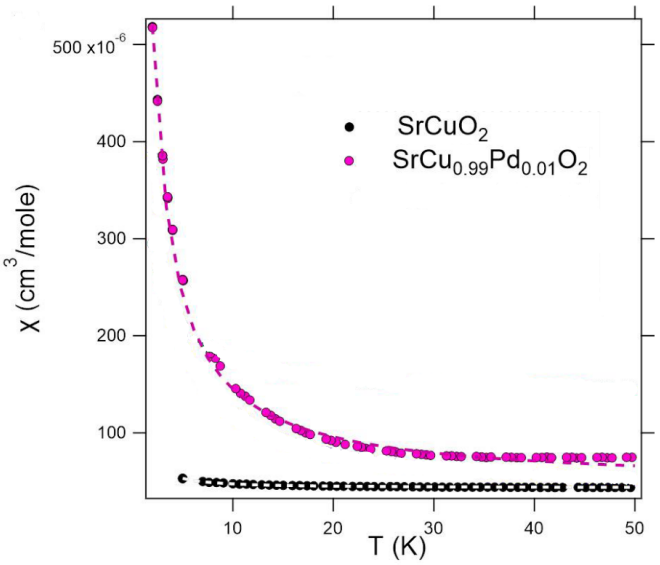

FIG. 6. DC Magnetic susceptibility of $SrCuO_2$ and $SrCu_{0.99}Pd_{0.01}O_2$ under a magnetic field of 1000 Oe applied along the spin chain axis c. The black dashed lines are the fit using the equation described in the text [36].

$g_{2\mathrm{ph}}$ is a new coupling constant $g_{2\mathrm{ph}} = C\ g_{1\mathrm{ph}}^2$ where C is a large number. At low temperature, this 2-phonons mean free path simply renormalizes single-phonon scattering; however, above ω^*, it introduces an extra power of T. In Figure 5, we show the thermal conductivity calcutated assuming these different approaches. The temperature dependence is quite similar, yet the coupling constants are chosen in the opposite strong and weak coupling limits. Our neutron study suggests that the weak coupling scenario should be preferred.

Appendix B: Effect of Pd doping on the spin chain

In this section, we envisage the effect of Pd doping in $SrCuO_2$ on the low energy sector of the two-spinons continuum. We confirm that controlled doping on the copper site depletes the low energy excitation spectrum. This gives a natural explanation for the strong reduction of spinon heat conductivity upon doping. Heat transport properties of cuprate spin chains are then ultimately much more sensitive to such local scatterers than to phonons. The Pd doping was introduced in the feed rod used in the TSFZM method, while the pellet used was pure CuO. The palladium content in the sample was verified by energy dispersive X-ray spectroscopy [34] , and gave the nominal composition of $SrCu_{0.99}Pd_{0.01}O_2$.

1. Characterisation of Pd doped sample

Different characterisation measurements have been first carried out on the Pd doped sample to determine the impact of the substitution on the spin chain and also estimate the super-exchange J_{AF}. A significant disruption could impact the exchange integral, to a point where the spin chain could be considered locally severed. To that end, two estimates of the super-exchange are given, from magnetic susceptibility and heat capacity measurements. The magnetic susceptibility measurements are reproduced below on Fig. 6. The susceptibility is fitted to a model proposed by Johnston [35, eq. 71] *et al.*

$$\chi(T) = \chi_0 + \chi_{CW} + \chi_s \tag{B1}$$

This expression is comprised of three terms. χ_0 is a constant in the temperature range considered, which contains the diamagnetic response of core electrons, and a paramagnetic response due to the deformation of the electron cloud induced by the magnetic field (Van Vleck contribution). χ_{CW} is the Curie-Weiss paramagnetic response, due to defects and unpaired spins. Finally χ_s is the intrinsic spin susceptibility, which contains the super exchange J_{AF}, as :

$$\chi_s = \frac{n_s(g\mu_B)^2}{J\pi^2}\left(1 + \frac{1}{2\ln(7.7J_{AF}/k_BT)}\right) \tag{B2}$$

In this expression, the second hand term is a logarithmic correction to the zero temperature limit of the spin susceptibility, due to Eggert [37] *et al.*, and is valid at temperatures below 10% of J_{AF}. n_s is the number of chains perpendicular to the (a,b) plane, which is 4 in the case of $SrCuO_2$. The resulting fits are reported on I.

Compared to the pure compound, the magnetic response of the spin chain is stronger at all temperatures,

Compound	C $(cm.K.mol^{-1})$	J_{AF} (K)	θ_{CW} (K)	χ_0 (cm.mol-1)
$SrCuO_2$	$3.9 \cdot 10^{-5} \pm 9.0 \cdot 10^{-7}$	2009 ± 200	1.09 ± 0.09	$4.3 \cdot 10^{-5} \pm 2.110^{-8}$
$SrCu_{0.99}Pd_{0.01}O_2$	$9.1 \cdot 10^{-4} \pm 2.8 \cdot 10^{-5}$	1700 ± 200	0.28 ± 0.05	$5.7 \cdot 10^{-5} \pm 8.2 \cdot 10^{-7}$

TABLE I. Resulting fits of data presented on 6 by B1.The standard error of parameters are reported [36].

even more so at low temperature. Breaking the spin chains induces lone 1/2 spins which raises the paramagnetic response encompassed in χ_0 (the Van Vleck contribution). The Curie constant increases as well, which is a concurring sign of an increased paramagnetic response.

From the fit results we observe a weak decrease of the super-exchange J_{AF} along the spin chain axis upon doping by Pd^{2+}. Upon doping by a Spin S=0 impurity, we showed before that the super-exchange is indeed slightly diminished [16]. The effective ionic radius of the Pd^{2+} ion is larger than Cu^{2+} in square planar configuration (64 pm vs. 62 pm, [38]). As the Pd^{2+} ion is larger that the dopants used before on the Cu^{2+} site, it is reasonable to expect a larger disturbance of the spin chain upon doping with a larger ion. As the dopant is larger, it also enlarges the lattice parameter b as revealed by X-ray powder scattering [36], but it did.

The heat capacity of $SrCu_{0.99}Pd_{0.01}O_2$ was measured with a magnetic field applied along the spin chain axis, and the result can be seen on 7. At high temperatures, the plot shows that the harmonic contribution to the heat capacity is much larger than the spin's. However, at low temperatures, the spin system attempts to order antiferromagnetically. As it was shown before [36], doping by a magnetic $S = 0$ impurity supresses the magnetic transition in those spin chains. Instead, at the expected ordering temperature, a large peak in the heat capacity is observed. In this system, the onset of the transition in visible down to 2K. The heat capacity is modeled at low temperatures as [39] :

$$C_p \approx \alpha T + \beta T^3 \tag{B3}$$

This model is comprised of a Debye term, the contribution from the crystalline lattice, which reduces to T^3 at low temperature. The Debye expression is valid for temperatures between 2 and $\Theta_D/50$ [40], where Θ_D is the Debye temperature. One can use the Pad approximant to the Debye term to fit a reasonable Debye temperature [41, eq. 13, table 2]. The Debye temperature is 250K in pure $SrCuO_2$ [39], which is extracted from a high temperature fit of the heat capacity. The linear term in the heat capacity model presented in B3 is due to the spin energy, and is related to super-exchange as [8, 35]:

$$\alpha = \frac{2\mathcal{N}_A k_B^2}{3J_{AF}} \tag{B4}$$

Here $\mathcal{N}_A$ is the Avogadro constant. This term is the magnetic contribution to the specific heat. It provides a second method to estimate the super-exchange of spin chains. From the fit of the heat capacity data, in the temperature range $[5^2-7^2]K^2$, we estimate $J_{AF} = 1930\pm$ 200K in $SrCu_{0.99}Pd_{0.01}O_2$ while we had $J_{AF} = 2060 \pm$ 100K in the pure compound, confirming the effect of the substitution by another measurement technique.

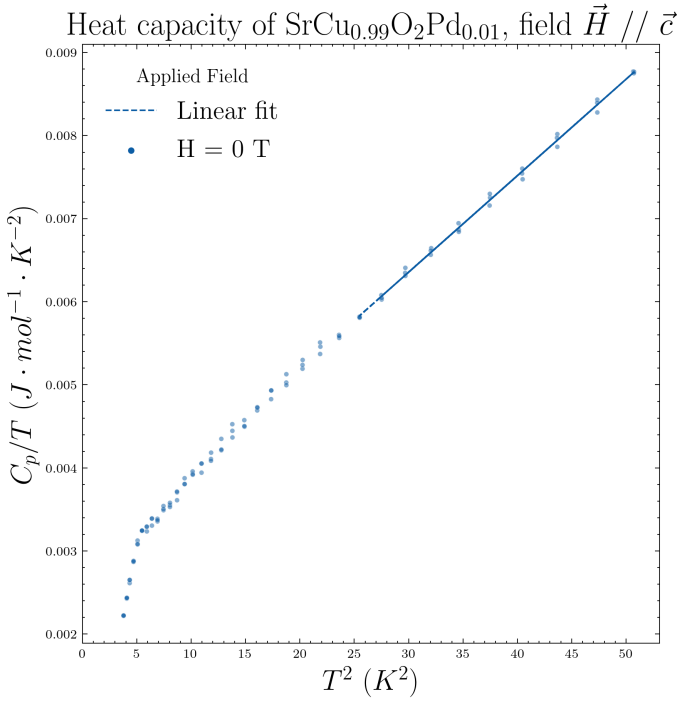

FIG. 7. Specific heat of $SrCu_{0.99}Pd_{0.01}O_2$, measured with applied magnetic field H along the spin chain axis c [36].

2. Neutron scattering results

Constant energy cuts were made through the 2-spinon continuum in the Pd doped sample $SrCu_{0.99}Pd_{0.01}O_2$. The scattered intensity is represented on8a), as a function of the neutron momentum exchange $\vec{Q} \parallel [10L]$ and the neutron energy exchange $\hbar\omega$. As the 2-spinon continuum is sharp along Q, the linewidth measured is merely the instrument resolution function convoluted with the samples mosaic. The resulting peak is thus approximated as a Gaussian lineshape, and the background is modeled by an affine function. The integrated area $\mathcal{S}(\omega)$ under the Gaussian was fitted by a phenomenological model

proposed by Simutis et al. [15]:

$$\mathcal{S}_\infty(\omega) = A\times\frac{(\gamma r_0)^2\, 2g^2}{4\pi J_{AF}}\frac{k_F}{k_i}\tanh\left(\frac{\hbar\omega}{2k_BT}\right)\cdot[n_B(T,\omega)+1]$$
$$F_{\Delta L}(\omega) = \left(\frac{\Delta_L}{2\hbar\omega}\right)^2 \sinh^{-2}\left(\frac{\Delta_L}{2\hbar\omega}\right)$$
$$\mathcal{S}(\omega) = \mathcal{S}_\infty(\omega)\times F_{\Delta_L}(\omega) \quad \text{(B5)}$$

In this expression, A=1.34 is the Mller ansatz, g is the Land g-factor, $(\gamma r_0)^2$=0.29 barn, J_{AF} is the superexchange, and $1+n_B$ is the detailed balance factor. The expression is the product of two parts. The function $\mathcal{S}_\infty$ represents the spin 1/2 infinite chain susceptibility [42], while the F_Δ function represents an envelope function. The spin pseudo-gap Δ suppresses the scattered intensity expected at $\omega = 0$; low energy spinons states are depleted, and no longer available for heat transport. This spin pseudo-gap also informs on the average chain length between dopants, scattered randomly in the crystal, on the Cu site. As the spinon continuum gets segmented by doping, an isolated spin chain of length L has an effective gap of $3.65J_{AF}/L$ [15]. Supposing a homogeneous and random spread of the dopant with concentration x, one can define a typical gap, the so-called pseudogap $\Delta = 3.65\cdot x/L$ and get information on the average chain length by fitting B5.

Each energy scan was fitted by a Gaussian lineshape of constant width, which encompasses the instrument resolution broadening, and the mosaic spread of the sample. The result of the fits is pictured on Fig.8. The resulting integrated area $\mathcal{S}_{1/2}(\omega)$ was then fitted by the expression given in B5. The fit of the integrated area yields Δ=12.0 meV with standard error of 1.6 meV. We observe on Fig.8 that after 8 meV, and around the 2-spinon continuum, the signal gets clouded by spurious signal, likely due to a low energy phonon branch, which is why the energy cuts were fitted between 2 and 8 meV in a tight Q-window.

We also performed a constant Q-scan at the position of the 2-spinon continuum and tried to fit the same model $\mathcal{S}(\omega)$. The gap extracted this way is 10.1 with standard error 2.4 meV. It was also fitted between 2 and 8 meV.

The fit yields the estimate of the spin pseudo-gap. It is worth noting that the spin pseudogap is higher than in $SrCuO_2$ doped with smaller ion in the spin chains. We attribute the larger spin pseudogap to the larger size of the palladium, which locally distorts the chain more significantly. This estimate can be compared to Nuclear Magnetic Resonance measurements [34], which report a spin pseudogap of 8.6 meV. The NMR probes the relaxation time between the spin and the lattice. An auxiliary transient AC magnetic field drives the ^{63}Cu nuclear spin to a high spin state, and the magnetization decay time informs on the coupling between the nuclear spin and its local surroundings. On the other hand, neutron scattering probes the global, unpaired electron spin-spin correlations in the material, and their onset above the spin pseudogap. The discrepancy could be explained by the different mechanisms governing the two measurements, as neutrons probe faster excitations than NMR.

[1] M. Li and G. Chen, Thermal transport for probing quantum materials, MRS Bulletin **45**, 348356 (2020).

[2] C. Hess, Heat conduction in low-dimensional quantum magnets, Eur. Phys. J. Spec. Top. **151**, 73 (2007).

[3] C. Hess, Heat transport of cuprate based low-dimensional quantum magnets with strong exchange coupling, Physics Reports **811**, 1 (2019).

[4] A. V. Sologubenko, K. Giannó, H. R. Ott, U. Ammerahl, and A. Revcolevschi, Thermal conductivity of the hole-doped spin ladder system sr14-xcaxcu24o41, Phys. Rev. Lett. **84**, 2714 (2000).

[5] A. V. Sologubenko, K. Giannò, H. R. Ott, A. Vietkine, and A. Revcolevschi, Heat transport by lattice and spin excitations in the spin-chain compounds $srcuo_2$ and sr_2cuo_3, Phys. Rev. B **64**, 054412 (2001).

[6] C. Hess, C. Baumann, U. Ammerahl, B. Büchner, F. Heidrich-Meisner, W. Brenig, and A. Revcolevschi, Magnon heat transport in $(Sr,Ca,La)_{14}cu_{24}o_{41}$, Phys. Rev. B **64**, 184305 (2001).

[7] H. Miike and K. Hirakawa, Evidence of the Diffusive Thermal Conduction in a One-Dimensional Antiferromagnet $KCuF_3$ above T_N ., Journal of the Physical Society of Japan **38**, 1279 (1975).

[8] A. V. Sologubenko, E. Felder, K. Giann, H. R. Ott, A. Vietkine, and A. Revcolevschi, Thermal conductivity and specific heat of the linear chain cuprate sr_2cuo_3 : evidence for thermal transport via spinons, Phys. Rev. B **62**, R6108 (2000).

[9] T. Kawamata, N. Takahashi, T. Adachi, T. Noji, K. Kudo, N. Kobayashi, and Y. Koike, Evidence for ballistic thermal conduction in the one-dimensional s=1/2 heisenberg antiferromagnetic spin system sr2cuo3, Journal of the Physical Society of Japan **77**, 034607 (2008).

[10] N. Hlubek, P. Ribeiro, R. Saint-Martin, A. Revcolevschi, G. Roth, G. Behr, B. Büchner, and C. Hess, Ballistic heat transport of quantum spin excitations as seen in $srcuo_2$, Phys. Rev. B **81**, 020405 (2010).

[11] N. Hlubek, P. Ribeiro, R. Saint-Martin, S. Nishimoto, A. Revcolevschi, S.-L. Drechsler, G. Behr, J. Trinckauf, J. E. Hamann-Borrero, J. Geck, B. Büchner, and C. Hess, Bond disorder and breakdown of ballistic heat transport in the spin-$\frac{1}{2}$ antiferromagnetic heisenberg chain as seen in ca-doped $\mathbf{srcuo_2}$, Phys. Rev. B **84**, 214419 (2011).

[12] N. Hlubek, X. Zotos, S. Singh, R. Saint-Martin, A. Revcolevschi, B. Bchner, and C. Hess, Spinon heat transport and spinphonon interaction in the spin-1/2 heisenberg chain cuprates sr_2cuo_3 and $srcuo_2$, Journal of Statistical Mechanics: Theory and Experiment **2012**, P03006 (2012).

[13] J. des Cloizeaux and J. J. Pearson, Spin-wave spectrum of the antiferromagnetic linear chain, Physical Review **128**, 2131 (1962).

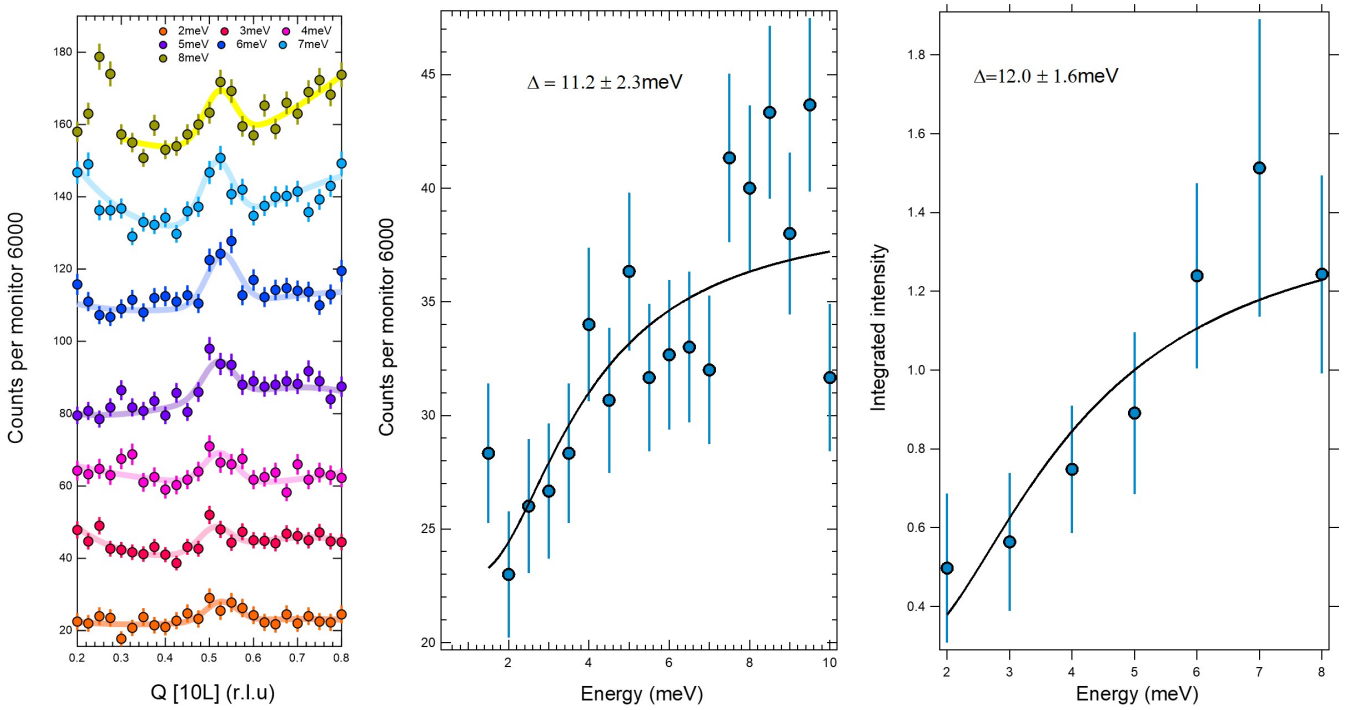

FIG. 8. (a) Scattered intensity of $SrCu_{0.99}Pd_{0.01}O_2$ around the 2-spinon continuum. (b) Neutron scattered intensity of $SrCu_{0.99}Pd_{0.01}O_2$, at position Q = 1 0 0.5 (reduced lattice units) at 3 K. The measurement was carried out with constant monitor (constant incoming neutron number at the sample), which is about 250s/point. (c) Integrated intensity $\mathcal{S}(\omega)$ as a function of the energy.

[14] B. Lake, D. A. Tennant, C. D. Frost, and S. E. Nagler, Quantum criticality and universal scaling of a quantum antiferromagnet, Nature Materials **4**, 329 (2005).

[15] G. Simutis, S. Gvasaliya, M. Mnsson, A. L. Chernyshev, A. Mohan, S. Singh, C. Hess, A. T. Savici, A. I. Kolesnikov, A. Piovano, T. Perring, I. Zaliznyak, B. Bchner, and A. Zheludev, Spin Pseudogap in Ni-Doped $SrCuO_2$, Phys. Rev. Lett. **111**, 10.1103/PhysRevLett.111.067204 (2013).

[16] D. Bounoua, R. Saint-Martin, S. Petit, P. Berthet, F. Damay, Y. Sidis, F. Bourdarot, and L. Pinsard-Gaudart, Impurity-induced spin pseudogap in srcuo$_2$ doped with mg, zn, or la, Phys. Rev. B **95**, 10.1103/PhysRevB.95.224429 (2017).

[17] X. Chen, J. Carrete, S. Sullivan, A. van Roekeghem, Z. Li, X. Li, J. Zhou, N. Mingo, and L. Shi, Coupling of spinons with defects and phonons in the spin chain compound ca$_2$cuo$_3$, Phys. Rev. Letters **122**, 10.1103/PhysRevLett.122.185901 (2019).

[18] E. Shimshoni, N. Andrei, and A. Rosch, Thermal conductivity of spin-$\frac{1}{2}$ chains, Phys. Rev. B **68**, 104401 (2003).

[19] A. L. Chernyshev and A. V. Rozhkov, Heat transport in spin chains with weak spin-phonon coupling, Phys. Rev. Lett. **116**, 017204 (2016).

[20] A. Revcolevschi, U. Ammerahl, and G. Dhalenne, Crystal growth of pure and substituted low-dimensionality cuprates $CuGeO_3$, La_2CuO_4, $SrCuO_2$, Sr_2CuO_3 and Sr14Cu24O41 by the floating zone and travelling solvent zone methods, Journal of Crystal Growth **198–199**, 593 (1999).

[21] J. Wada, S. Wakimoto, S. Hosoya, K. Yamada, and Y. Endoh, Preparation of single crystal of Ca_2CuO_3 by TSFZ method, Physica C: Superconductivity **244**, 193 (1995).

[22] D. Msika, D. Bounoua, F. Damay, A. Ivanov, S. Petit, L. Pinsard-Gaudart, A. Piovano, and R. Saint-Martin, *Lattice Dynamics of the Low-Dimensional Sr_2CuO_3* (Institut Laue-Langevin (ILL), 2019).

[23] D. Msika, D. Bounoua, F. Damay, A. Ivanov, S. Petit, L. Pinsard-Gaudart, and R. Saint-Martin, *High Energy Spinon-phonon Coupling in Spin Chain Cuprates* (Institut Laue-Langevin (ILL), 2020).

[24] D. Bounoua, F. Damay, M. Enderle, D. Msika, S. Petit, L. Pinsard-Gaudard, R. Saint-Martin, and T. Weber, *Spinon-Phonon Interaction in the Low-Dimensional $SrCuO_2$* (Institut Laue-Langevin (ILL), 2018).

[25] I. A. Zaliznyak, H. Woo, T. G. Perring, C. L. Broholm, C. D. Frost, and H. Takagi, Spinons in the strongly correlated copper oxide chains in srcuo$_2$, Phys. Rev. Lett. **93**, 10.1103/physrevlett.93.087202 (2004).

[26] S. Baroni, S. de Gironcoli, A. Dal Corso, and P. Giannozzi, Phonons and related crystal properties from density-functional perturbation theory, Reviews of Modern Physics **73**, 515 (2001).

[27] Meyer, Elsasser, Lechermann, and Fahnle, Fortran90 program for mixed-basis pseudopotential calculations for crystals.

[28] R. Heid and K.-P. Bohnen, Linear response in a density-functional mixed-basis approach, Physical Review B **60**, R3709 (1999).

[29] D. Vanderbilt, Optimally smooth norm-conserving pseudopotentials, Physical Review B **32**, 8412 (1985).

[30] J. P. Perdew and Y. Wang, Accurate and simple analytic representation of the electron-gas correlation energy, Physical Review B **45**, 13244 (1992).

[31] M. d Astuto and M. Krisch, High resolution inelastic X-ray scattering from thermal collective excitations (EDP Sciences, 2010) pp. 487–503.

[32] S. Sugai, J. Wada, K. Yamada, S. Hosoya, and Y. Endoh, Spin-phonon interactions in the raman spectra of one- and two-dimensional quantum spin antiferromagnets, Physica B: Condensed Matter **219-220**, 505 (1996), pHONONS 95.

[33] M. Aïn, J. E. Lorenzo, L. P. Regnault, G. Dhalenne, A. Revcolevschi, B. Hennion, and T. Jolicoeur, Double gap and solitonic excitations in the spin-peierls chain $cugeo_3$, Phys. Rev. Lett. **78**, 1560 (1997).

[34] Y. Utz, F. Hammerath, R. Kraus, T. Ritschel, J. Geck, L. Hozoi, J. van den Brink, A. Mohan, C. Hess, K. Karmakar, S. Singh, D. Bounoua, R. Saint-Martin, L. Pinsard-Gaudart, A. Revcolevschi, B. Bchner, and H.-J. Grafe, Effect of different in-chain impurities on the magnetic properties of the spin chain compound $SrCuO_2$ probed by NMR, Phys. Rev. B **96**, 115135 (2017).

[35] D. C. Johnston, R. K. Kremer, M. Troyer, X. Wang, A. Klmper, S. L. Budko, A. F. Panchula, and P. C. Canfield, Thermodynamics of spin s=1/2 antiferromagnetic uniform and alternating-exchange heisenberg chains, Phys. Rev. B **61**, 9558 (2000).

[36] D. Bounoua, *Synthse et tudes de cuprates de basse dimensionnalit a proprits thermiques fortement anisotropes* (Thse de l'Universit Paris Sud, 2017).

[37] S. Eggert, I. Affleck, and M. Takahashi, Susceptibility of the spin 1/2 heisenberg antiferromagnetic chain, Phys. Rev. Lett. **73**, 332 (1994).

[38] R. D. Shannon, Revised effective ionic radii and systematic studies of interatomic distances in halides and chalcogenides, Acta Crystallographica Section A: Crystal Physics, Diffraction, Theoretical and General Crystallography **32**, 751 (1976).

[39] P. Ribeiro, *One-Dimensional Quantum Magnets in Cuprates: Single Crystal Growth and Magnetic Heat Transport Studies* (Phd thesis, Dresden, 2007).

[40] G. R. Stewart, Measurement of lowtemperature specific heat, Review of Scientific Instruments **54**, 1 (1983).

[41] R. J. Goetsch, V. K. Anand, A. Pandey, and D. C. Johnston, Structural, thermal, magnetic, and electronic transport properties of the $LaNi_2(ge_{1-x}p_x)_2$ system, Phys. Rev. B **85**, 054517 (2012).

[42] G. Mller, H. Thomas, H. Beck, and J. C. Bonner, Quantum spin dynamics of the antiferromagnetic linear chain in zero and nonzero magnetic field, Phys. Rev. B **24**, 1429 (1981).